Anal. Chem. **2000,** *72,* 4255−4265

Modeling Interparticle and Intraparticle (Perfusive) Electroosmotic Flow in Capillary Electrochromatography

Patrick T. Vallano and Vincent T. Remcho*

Department of Chemistry, Oregon State University, Corvallis, Oregon 97331-4003

A model to estimate the extent of intraparticle, or perfusive, electroosmotic flow (EOF) in CEC capillaries packed with macroporous particles has been developed. Nucleosil packings (d_p= 7 μm) having nominal pore sizes of 500, 1000, and 4000 Å were studied. Intraparticle pores ranging from 50 to 10 000 Å in diameter were partitioned into 995 intervals of 10 Å. Using pore size distribution data for the sorbents obtained by mercury intrusion porosimetry, fractions of the total column void volume contributed by pores in the range of interest were determined. The average channel diameter of the interstitial space was estimated from the d_p of the packing; its fraction of total column volume was determined from the interstitial porosity. Estimations of relative EOF velocity in the intraparticle and interstitial channels were made by treating the channels as parallel cylindrical capillary tubes. Relative EOF values were combined with the volume fraction data and used as weighting factors in calculating an effective particle diameter ($d_{p,eff}$) for each set of conditions (i.e., packing type, ionic strength of eluent). Values of $d_{p,eff}$ generated by the model correctly predict the trends observed in the experimental data. At the lowest ionic strength, plate height correlated inversely with the pore size of packing ($h_{4000\ Å} < h_{1000\ Å} < h_{500\ Å}$). Rate curves for each column tended toward lower plate heights with increasing eluent ionic strength before converging at some limiting point. The point of convergence was reached at moderate ionic strengths for the larger pore media (1000 and 4000 Å) and higher ionic strength for the 500 Å.

One of the reasons capillary electrochromatography (CEC) has garnered the attention of many separation scientists over the past decade or so [1−5] is the technique's efficiency advantage relative to HPLC. The motive force for bulk flow in CEC is electroosmosis, the flow dynamics of which yield lower plate heights when compared to capillary HPLC in a given column. In CEC, electroosmotic flow (EOF) velocity is, within limits, defined by double-layer thickness and Joule heating, radially uniform across a given flow channel and independent of channel diameter. As a result of these enhanced flow properties, sources of peak dispersion arising from nonuniformity in flow velocity, specifically eddy diffusion and mobile-phase mass-transfer effects, are generally smaller in CEC than HPLC, as is overall plate height.

Chromatographic rate theory predicts lower plate heights when smaller diameter packing particles are employed.[6] For this reason, practitioners of HPLC generally employ the smallest particles practically possible (usually 3−5 μm in diameter). This maxim holds for CEC as well. In contrast to HPLC, the absence of pressure drop imposes no limit on the use of submicrometer particles in CEC, which in principle should provide maximum efficiency. This approach has yielded promising results,[7,8] though it presents a number of practical limitations. Chief among these are difficulties in column preparation due to the small particle size and a lack of commercial availability of the particles.

Macroporous packings present an alternative pathway to improving efficiency in CEC because, under the proper conditions, the macropores in such particles can support EOF.[9] Widely available from a number of manufacturers, these particles are typically larger in diameter (e.g., 5−10 μm) with mean pore diameters above 500 Å. As are most typical silica-based HPLC packings, macroporous particles are corpuscular in nature, produced by sol−gel methods in which colloidal silica particles ("microbeads") coalesce under controlled conditions to form porous spheres composed of agglomerates of microbeads.[10] Pore size can be adjusted by altering the size of the silica sol particles and their packing density. One advantage that immediately accrues to the use of these media is the relative ease of capillary packing. The practical complications associated with packing submicrometer particles, clogging, for example, are avoided. Additionally, larger diameter particles can be well packed using conventional slurry packing methods.

In the "through-pore", or perfusive EOF regime, analyte molecules in the mobile phase sample two distinct regions of space, that between packing particles (the interstitial space) and

(1) Knox, J. H.; Grant, I. H. *Chromatographia* **1987**, *24*, 135−143.
(2) Knox, J. H.; Grant, I. H. *Chromatographia* **1991**, *32*, 317−328.
(3) Dittmann, M. M.; Wienand, K.; Bek, F.; Rozing, G. P. *LC-GC* **1995**, *13*, 802−814.
(4) Crego, A. L.; González, A.; Marina, M. L. *Crit. Rev. Anal. Chem.* **1996**, *26*, 261−304.
(5) Vallano, P. T.; Remcho, V. T. *J. AOAC Int.* **1999**, *82*, 1604−1612.
(6) Giddings, J. C. *Dynamics of Chromatography*; Marcel Dekker: New York, 1965.
(7) Lüdtke, S.; Adam, T.; Unger, K. K. *J. Chromatogr., A* **1997**, *786*, 229−235.
(8) Reynolds, K. J.; Colón, L. A. *J. Liq. Chromatogr. Relat. Technol.* **2000**, *23*, 161−173.
(9) Li, D.; Remcho, V. T. *J. Microcolumn Sep.* **1997**, *9*, 389−397.
(10) Unger, K. K. *Porous Silica*; Elsevier: Amsterdam, 1979; Chapter 2.

10.1021/ac0005969 CCC: $19.00
Published on Web 08/11/2000

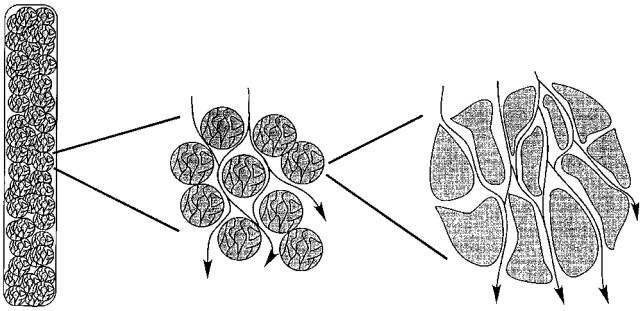

Figure 1. Schematic representation of interparticle and intraparticle flow in a packed CEC column. Arrows indicate mobile-phase stream paths.

the spaces in the pores of the particles (the intraparticle region). This is depicted schematically in Figure 1. In the interstitial space, flow channel diameter is proportional to the diameter of the packing particle (d_p). For this reason, individual sources of flow velocity inhomogeneity (with the associated diffusion distances, persistence of velocity spans, etc.) are scaled to particle diameter.[6] The flow channel diameter in the intraparticle region is independent of d_p and instead is a function of the diameter of microbeads constituting the particle. Under conditions such that a considerable fraction of the total column flow occurs through the particles, the *effective* particle diameter $d_{p,eff}$, which is dictated to a large extent by the microbead diameter, will therefore be lower than d_p.

In addition to a smaller effective particle diameter, operating in a perfusive EOF mode provides a further advantage in that a substantially lower contribution of stagnant mobile-phase mass transfer to plate height is expected. With conventional small-pore media, fluid occupying the pores is generally stagnant. Broadening of the analyte zone occurs due to slow diffusion between the stagnant and mobile fluids and is greater in magnitude at higher flow velocities. This phenomenon manifests itself as an increasingly positive slope on the high-velocity side of plate height versus linear velocity (rate) curves. In a perfusive system, however, the fluid in much of the pore space is no longer stagnant and the system takes on the characteristics of a bed composed of small-diameter, essentially nonporous particles, which are ideal from the standpoint of efficiency.

Recent studies on the use of macroporous packings in CEC have demonstrated the predicted improvements in efficiency brought about by intraparticle EOF.[9,11] Using 7 μm d_p, 4000 Å pore Nucleosil C18 particles, Stol et al.[11] observed plate heights only slightly greater than those generated with 1.5 μm nonporous particles. Reduced plate heights as low as 0.34 were obtained for fluorene.

When assessing column performance, reduced parameters are recommended[6,12] in which plate height is scaled to d_p. In the perfusive EOF regime, however, reduced parameters calculated by scaling to d_p are not representative because the "effective" particle diameter is less than d_p. On this basis, it would be useful to devise a method by which the effective particle diameter for a given set of conditions could be estimated. Although the effective particle diameter has no physical meaning, such a parameter would allow for (1) more accurate scaling of plate height and velocity, thus facilitating comparisons of different conditions and determinations of plate height coefficients, and (2) estimation of the gain in efficiency as the perfusive character of the packings is increased. In this paper, a model has been developed by which the extent of intraparticle flow in CEC columns packed with different pore sizes of macroporous particles was estimated for a range of eluent ionic strengths. By means of the model, an effective particle diameter was obtained for each test condition. The values generated predict the observed trends in the experimental data.

THEORY

As has been well-documented,[13] the electrical double layer, which forms near charged surfaces, gives rise to electroosmotic flow. In CEC with conventional sorbents, electrical double-layer formation is the result of a net negative charge present at the surface of the silica packing particles and the capillary wall. Application of an electric potential gradient along the capillary axis causes mobile ions in the double layer to migrate resulting in EOF. Rice and Whitehead[14] published a thorough treatment of EOF in cylindrical capillary tubes in which EOF velocity V was shown to be a function of radial position in the tube r described as follows:

$$V(r) = \frac{\epsilon_0 \epsilon r \zeta E}{\eta}\left[1 - \frac{I_0(\kappa r)}{I_0(\kappa a)}\right] \qquad (1)$$

where ϵ_0 is the permittivity of vacuum, ϵ_r is the dielectric constant of the solution, ζ is the zeta potential (the potential at the shear plane), E is the applied electric field strength, η is the solution viscosity, I_0 is a zero-order modified Bessel function of the first kind, κ is the reciprocal of the electrical double-layer thickness, r is the distance from the tube center, and a is the tube diameter. The double-layer "thickness" δ is the distance (from the wall) at which the potential decays to $1/e$, or 0.37 of its value at the wall and for a (1:1) univalent electrolyte is given by

$$\delta = \kappa^{-1} = \left(\frac{\epsilon_0 \epsilon_r RT}{2CF^2}\right)^{1/2} \qquad (2)$$

in which R is the universal gas constant, T is absolute temperature, C is the molar concentration of electrolyte, and F is Faraday's constant. Apparent in eq 2 is the inverse square root relationship between double-layer thickness and electrolyte concentration. The electrokinetic radius, κa, is the ratio of channel radius to double-layer thickness.

Under conditions in which the flow channel diameter is large relative to the double-layer thickness, typical in CEC, the term in brackets in eq 1 approaches zero and the expression reduces to the familiar Smoluchowski equation in which V is essentially independent of radial position in the channel.

$$V = \epsilon_0 \epsilon_r \zeta E / \eta \qquad (3)$$

However, in narrow flow channels (e.g., in the pores of the packing material), values of κa will be much smaller than in the interstitial

(11) Stol, R.; Kok, W. T.; Poppe, H. *J. Chromatogr., A* **1999**, *853*, 45−54.
(12) Knox, J. H.; Kennedy, G. *J. Chromatgr. Sci.* **1972**, *10*, 549−556.
(13) Hunter, R. J. *Zeta Potential in Colloid Science*; Academic Press: London, 1981; Chapters 2−3.
(14) Rice, C. L.; Whitehead, R. *J. Phys. Chem.* **1965**, *69*, 4017−4024.

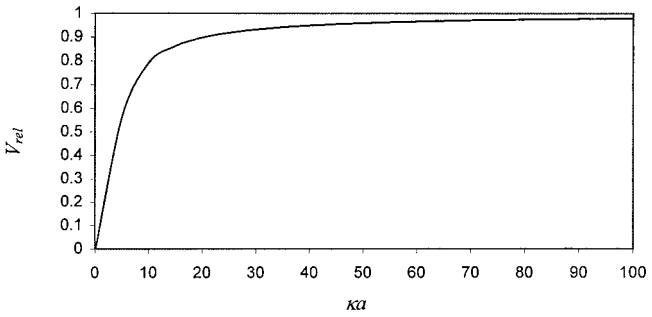

Figure 2. Relative EOF velocity as a function of electrokinetic radius (κa).

channels and the term in brackets in eq 1 must be considered. A useful parameter with which to evaluate V in such conditions is the relative EOF velocity V_{rel},[15] which is derived as follows. From eq 1, the cross sectional average velocity can be obtained:

$$\bar{V} = \frac{\epsilon_0 \epsilon_r \xi E}{\eta}\left[1 - \frac{2I_1(\kappa a)}{\kappa a I_0(\kappa a)}\right] \tag{4}$$

where I_1 is a first-order modified Bessel function of the first kind. For $\kappa a \gg 1$, the term in brackets in eq 4 approaches unity, and expressions 3 and 4 become equivalent. If, for clarity, the average velocity at large κa is expressed as $\bar{V}_\infty$, then the relative EOF velocity, V_{rel} is given by

$$V_{rel} = \frac{\bar{V}}{V_\infty} = \left[1 - \frac{2I_1(\kappa a)}{\kappa a I_0(\kappa a)}\right] \tag{5}$$

Figure 2 is a plot of V_{rel} versus κa, which helps to illustrate the salient features of eq 5. Although, for finite values of κa, $V_{rel} < 1$, there is an asymptotic approach toward unity such that, at large κa (>50), V_{rel} is essentially equal to $\overline{V_\infty}$, hence the validity of the Smoluchowski equation. In contrast, for $\kappa a < 10$, a sharp dependence of V_{rel} on κa is observed.

Model Design. The goal of this study was to develop a model that could be used to estimate the contribution of intraparticle EOF to the total flow in the packed column for a given nominal pore size of packing and eluent ionic strength. To that end, a model was designed in which a weighted average channel diameter was determined for a column under a given set of operating conditions. In addition to the interstitial space, intraparticle pores with diameters in the range 50−10 000 Å, readily determinable by mercury intrusion porosimetry, were considered. An overview of the model is as follows. Initially, the fraction of total void space in the column accessible by the mobile phase, the total column porosity, was estimated. The intraparticle pores under consideration were then partitioned into intervals of 10 Å. Using pore size distribution data for the packings obtained by mercury intrusion porosimetry, the volume fraction for each interval (i.e., its fraction of the total column void space) was determined. In a similar manner, the volume fraction of the interstitial space was estimated. Next, the relative magnitude of EOF velocity in each channel diameter interval was estimated by treating the channels as parallel cylindrical capillary tubes of equal length. With this assumption, relative EOF velocity was determined using the well-known Rice and Whitehead relationships, in which EOF velocity is a function of κa in the channel. The volume fractions and estimations of relative EOF velocity, calculated for each of the 10 Å intervals representing the intraparticle region and for the interstitial region, were used as weighting factors in calculating an average flow channel diameter for a given set of conditions. The average *channel* diameter obtained from the model was subsequently converted to an average effective *particle* diameter to enable a more facile interpretation of the results.

Calculation of Weighting Factors. Pore size distributions for the different nominal pore diameter Nucleosil packings were determined by mercury intrusion porosimetry. Pore diameters from 50 to 10 000 Å were partitioned into 995 intervals, each spanning 10 Å. Using the porosimetry data, a given interval's fraction of the total pore volume f_i was calculated by determining the fraction of the total area under the pore size distribution curve contributed by the interval.

$$f_i = \left(\frac{\text{interval volume}}{\text{cumulative pore volume}}\right) \tag{6}$$

The 10 Å interval i was then assigned a nominal pore (channel) diameter d_{ch} equal to the midpoint of the interval. For example, if pores between 270 and 280 Å in diameter constituted 1% of the total pore volume, then the volume contribution was considered to arise from 275 Å pores (i.e., $d_{ch} = 275$ Å). In this way, the pore size distribution data were discretized with the large number of intervals ensuring minimal loss of coherence.

The fraction of void space in the column occupied by the mobile phase, ϵ_{tot} is given by

$$\epsilon_{tot} = \epsilon_i + \epsilon_p(1 - \epsilon_i) \tag{7}$$

where ϵ_i is the fraction of interstitial free space in the column (the interstitial porosity) and ϵ_p is the particle porosity. The fraction of total column void space contributed by the pores of the packing particles is then

$$\epsilon_{pore} = \epsilon_p(1 - \epsilon_i)/\epsilon_{tot} \tag{8}$$

For well-packed chromatographic columns, ϵ_i is typically on the order of 0.4 [6] and eq 8 reduces to $\epsilon_{pore} = 0.6(\epsilon_p/\epsilon_{tot})$. Values of ϵ_p for the Nucleosil materials were obtained from the porosimetry data. The fraction of total column void space contributed by the packing interstices is $1 - \epsilon_{pore}$.

For the intraparticle pores, the volume fraction weighting factor χ_v for a given 10 Å pore diameter interval i is defined as the fraction of total column volume contributed by interval i. The sum of χ_v over all intervals is therefore equal to ϵ_{pore}.

$$\chi_v \text{ (interval } i) = (f_i)(\epsilon_{pore}) \tag{9}$$

$$\sum_{i=1}^{i=995} \chi_v i = \epsilon_{pore} \tag{10}$$

The volume fraction weighting factor for the interstitial channels is $1 - \epsilon_{pore}$.

(15) Wan, Q.-H. *Anal. Chem.* **1997**, *69*, 361−363.

The relative EOF velocity weighting factor, χ_e for pore interval i is equal to the relative EOF velocity for a cylinder of the appropriate diameter, given by eq 5

$$\chi e(i) = \left[1 - \frac{2I_1(\kappa a_i)}{\kappa a I_0(\kappa a_i)}\right] \tag{11}$$

in which a_i is the nominal pore radius (0.5 d_{ch}) of the interval. The value of κ is dependent upon the ionic strength of the eluent. For the interstitial space, the channel radius a was estimated from the particle diameter d_p and the interstitial porosity using the following relationship.[16]

$$a = 0.21\, d_p\left(\frac{\epsilon_i}{1-\epsilon_i}\right) \tag{12}$$

Weighted Average Particle Diameter. To calculate a weighted average particle diameter, χ_v and χ_e were combined into a single lumped weighting factor χ_l for each channel under consideration.

$$\chi_l\,(i) = [\chi_v(i)][\chi_e(i)] \tag{13}$$

An average channel diameter $\overline{d_{ch}}$ was subsequently obtained by calculating the weighted average of the individual flow channels

$$\overline{d_{ch}} = \frac{\begin{array}{c}\text{intraparticle}\\ \text{contribution}\\ (\chi_l 1)(d_{ch}1)\end{array} + \ldots + (\chi_l 995)(d_{ch}995) + \begin{array}{c}\text{interstitial (int)}\\ \text{contribution}\\ (\chi_l \text{int})(d_{ch}\text{int})\end{array}}{\chi_l 1 + \chi_l 995 + \chi_l \text{int}} \tag{14}$$

Rearranging eq 12 and once again setting $\epsilon_i = 0.4$, $\overline{d_{ch}}$ was converted to an effective particle diameter $d_{p,eff}$

$$d_{p,eff} = 3.57\overline{d_{ch}} \tag{15}$$

The effective particle diameter for a given type of packing is dependent upon the pore size distribution of the material, its porosity, and the ionic strength of the eluent. At lower ionic strengths, where the double-layer thickness δ is large relative to the mean pore diameter of the packing (small κa), a larger $d_{p,eff}$ is predicted. As ionic strength is increased, a greater fraction of the pores can support EOF, resulting in a lower $d_{p,eff}$. In contrast to the macroporous particles employed in this study, conventional (e.g., 60−80 Å pore diameter) HPLC packings in general possess an insufficient fraction of pores large enough to support EOF. With such particles, the interstitial contribution dominates eq 14 and $d_{p,eff} \approx d_p$. Alternatively, if a packing were employed having a uniform distribution of macropores in which vigorous electroosmosis could occur, a limiting value of $d_{p,eff}$ would be reached because the intraparticle pore space in a typical column constitutes only 40−50% of the total volume accessible to the mobile phase. The remaining fraction arises from the interstitial space. In practice, the relatively broad pore size distributions of many macroporous packings, which often include a fraction of mesopores (<500 Å), impose more stringent limits on the minimum achievable value of $d_{p,eff}$.

In the work presented here, commercially available macroporous silica HPLC packings (Nucleosil, Macherey-Nagel, Duren, Germany) of three different nominal pore diameters were examined using typical CEC eluents with a range of ionic strengths. An unretained test probe, acetone, was employed to monitor plate height as a function of eluent ionic strength. The model described above was used to estimate $d_{p,eff}$ for each combination of packing and eluent ionic strength. Values of $d_{p,eff}$ obtained from the model were then used to reconstruct experimental reduced plate height versus reduced velocity plots.

EXPERIMENTAL SECTION

Materials and Reagents. Concentrated hydrochloric acid (37%) and HPLC grade acetone were purchased from Mallinckrodt, St. Louis, MO. Ultrapure grade (99.9+%) tris(hydroxymethyl)aminomethane (Tris) was obtained from Aldrich Chemical, Milwaukee, WI. HPLC grade acetonitrile was purchased from Fisher Scientific, Pittsburgh, PA. All water used in this study was filtered and deionized using a Barnstead Series 582 water purification system (Barnstead/Thermolyne Corp., Dubuque, IA). Fused-silica capillary tubing of 75 μm i.d., 360 μm o.d., was purchased from Polymicro Technologies, Inc., Phoenix, AZ. Nucleosil C18 silica particles (d_p = 7 μm) with nominal pore diameters of 300, 500, 1000, and 4000 Å were obtained from Meta Chem Technologies, Torrance, CA.

The desired concentrations of Tris buffer were obtained by first preparing a 500 mM stock solution of Tris (base form) and subsequently diluting in deionized H_2O to 100 mM. The pH of this 100 mM solution was adjusted to 8.0 by titration with concentrated HCl, after which dilutions were performed to yield 75, 50, 25, 10, and 1.0 mM buffer solutions. The concentration of protonated Tris (acid form), necessary for double-layer thickness calculations, was estimated using the Henderson−Hasselbach equation. Appropriate volumes of each buffer were mixed with acetonitrile to yield (20:80) (v/v) buffer/acetonitrile solutions, which were then employed as eluents in the capillary electrochromatography experiments. In this system, ionic strength I is essentially equal to the concentration of Tris in the acid form. It should be noted that the various Tris concentrations employed in this study are identified herein according to their nominal values, i.e., the total concentration of Tris in the aqueous component of the mobile phase (1, 10, 25, 50, 75, and 100 mM). In calculating values of δ, however, the final concentration of ionized Tris (determined as described above and accounting for the 1:5 v/v dilution in acetonitrile) was used.

Capillary Columns. The initial step in capillary preparation was the formation of a frit to retain the particles during packing. After cutting to the desired length, one end of the capillary tube was tapped into dry packing material until the material protruded a short distance into the tube. The packing material was sintered by heating with an electric arc fusion splicer (Alcoa Fujikura, Tokyo, Japan). A slurry was made by suspending 10 mg of particles in 1.0 mL of acetonitrile. Using an Isco 100 DX syringe pump (Isco, Inc., Lincoln, NE) with 50% (v/v) acetonitrile/water as the packing solvent, the particles were forced into the capillary

(16) Wan, Q.-H. *J. Phys. Chem. B* **1997**, *101*, 4860−4862.

Table 1. Physical Dimensions of Capillary Columns Used in This Study

packing type (Nucleosil C18)				
d_p (μm)	pore diameter(Å)	i.d. (μm)	L_{bed} (cm)	L_{tot} (cm)
7	500	75	24.0	32.5
7	1000	75	24.0	32.6
7	4000	75	24.1	32.6

tube by applying an initial pressure of 1000 psi after which the pressure was increased gradually to 3500 psi. When the packed bed reached at least 25 cm, a second frit was made ~24 cm from the first frit, again by sintering with the fusion splicer. After sintering, the pump was stopped and the pressure slowly allowed to decay to zero. Finally the capillary was reverse flushed (i.e., with the original frit at the inlet) in order to expend the loose packing (downstream from the outlet) from the column. The section of capillary immediately downstream from the outlet frit served as the detection window. It was necessary to use a sharp knife to scrape away some of the polyimide cladding a short distance downstream from the frit in order to provide a fully unobstructed window for detection. The distance from the outlet frit to the point of detection was 1 mm or less for each column. The dimensions of the columns employed in this study are summarized in Table 1.

Capillary Electrochromatography. All CEC runs were conducted on a Hewlett-Packard ^{3D}CE instrument (Hewlett-Packard Co., Waldbronn, Germany) equipped for external pressurization. The instrument's standard photodiode array detector was used to monitor the UV absorbance of acetone at 280 nm. External pressure, typically 5 bar, was applied to the inlet and outlet mobile-phase vials in all CEC experiments to minimize bubble formation. The capillary temperature was held at 25 °C. Acetone samples were prepared for each experiment by diluting HPLC grade acetone (1:10, v/v) in the appropriate mobile phase and injected electrokinetically (+5 kV, 3 s) onto the column. To minimize the possibility of sample focusing, the mobile phase used to prepare the acetone sample was identical to that used for the analysis. The retention time of acetone, an unretained compound with no net electrophoretic mobility, was used to estimate the mobile-phase linear velocity, μ. An approximate value for the diffusion coefficient for acetone in the mobile phase D_m was obtained using the Wilke−Chang equation ($D_m = 3.1 \times 10^{-5}$ cm^2 s^{-1}). Data points presented in the text represent the mean retention time value for three replicate injections.

Physical Characterization of Nucleosil Packing Materials. Pore size distributions of the Nucleosil packing materials were investigated by mercury intrusion porosimetry. These analyses were performed by Micromeritics, Norcross, GA, using a Micromeritics AutoPore mercury porosimeter. Scanning electron microscopy (SEM) images of the packings were obtained using an AmRay 3300 FE scanning electron microscope (AmRay, Bedford, MA).

Data Analysis. Chromatographic data were collected and processed using the Hewlett-Packard ChemStation software (Hewlett-Packard Co.), standard equipment on the instrument. Rate curves and others graphs were prepared with Microsoft Excel (Microsoft Corp., Renton, WA). Analysis of the porosimetry data was performed using GraphPad Prism (GraphPad Software, Inc., San Diego, CA).

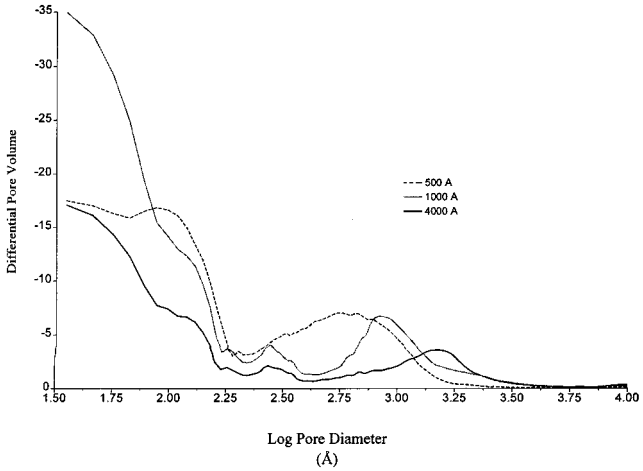

Figure 3. Pore size distributions of Nucleosil packings determined by mercury intrusion porosimetry.

Table 2. Physical Characteristics of Nucleosil Packings Determined by Mercury Intrusion Porosimetry

nominal pore diameter (Å)	cumulative pore volume (mL g^{-1})	ϵ_p	median pore diameter (Å)
500	0.8820	0.69	620
1000	1.049	0.80	980
4000	0.7971	0.69	1580

RESULTS/DISCUSSION

Characterization of the Nucleosil Particles. The pore size distributions of the Nucleosil particles obtained by mercury porosimetry are shown in Figure 3. Each material exhibited a broad, bimodal distribution, with a maximum at ~120 Å (mesopores) and another at some larger diameter (macropores), the exact value of which depended on the material. The second maxima in the distributions occur at approximately 600, 800, and 1600 Å, respectively, for the 500, 1000, and 4000 Å (quoted) nominal pore sizes. These distributions show that although all the packings possess some amount of macropores (greater than 500 Å in diameter), expectedly the 1000 and 4000 Å media contain greater fractions of the largest pores (above 1500 Å). The characteristics of these pore size distributions are quite important in accounting for the observed chromatographic behavior of these packing materials. The physical parameters gleaned from the porosimetry analyses of these materials are summarized in Table 2.

These results are in agreement with those previously reported for 5 μm d_p macroporous Nucleosil particles performed by Tanaka et al.[17] Through mercury intrusion porosimetry and electron microscopy analyses, these workers showed that each nominal pore size of packing tested consisted of a mixture of different particles, each having distinct pore sizes and structures.

Scanning electron micrographs of the particles provided some useful insight into the pore structures of the packings used in

(17) Tanaka, N.; Hashidzume, K.; Araki, M.; Tsuchiya, H.; Okuno, A.; Iwaguchi, K.; Ohnishi, S.; Takai, N. *J. Chromatogr.* **1988**, *448*, 95−108.

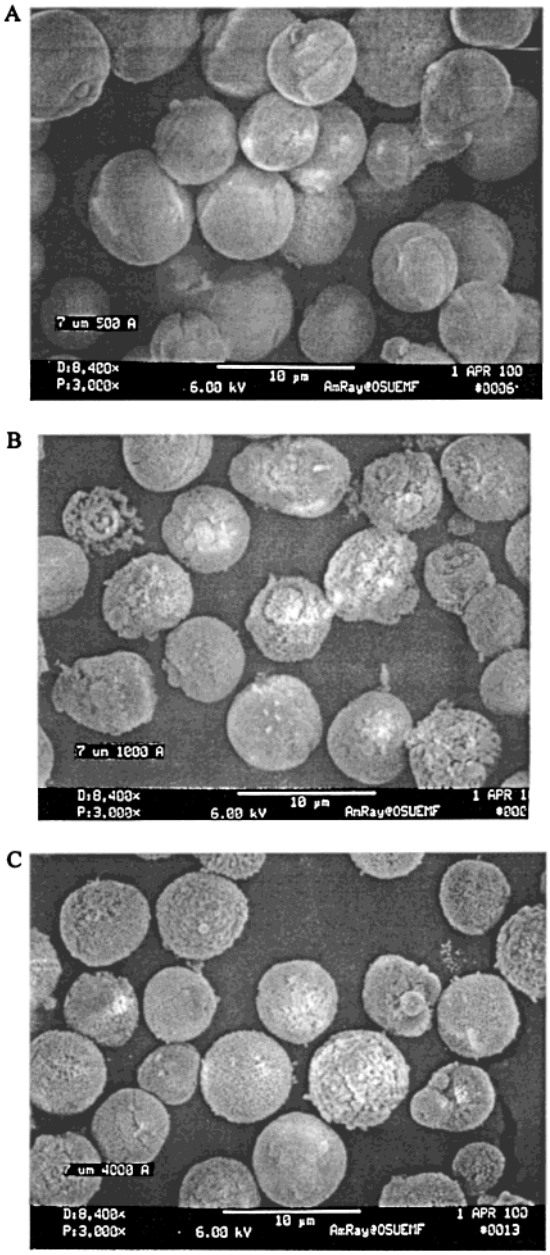

Figure 4. Scanning electron micrographs of Nucleosil packings employed in this study. (A) 500 Å, (B) 1000 Å, (C) 4000 Å mM Tris.

this study. Images obtained for the 500, 1000, and 4000 Å nominal pore sizes are presented in Figure 4 A−C, respectively. The corpuscular structure of these media, as well as the different types of particles present, is evident in these images. The preponderance of macroporous particles in the 1000 and 4000 Å packings, relative to the 500 Å, is clearly visible. In agreement with the porosimetry data, the 4000 Å packing (Figure 4C) appears to possess the greatest fraction of the largest pore size particles.

Transmission electron micrographs of 5 μm d_p Nucleosil particles [17] better illustrate the characteristic pore structures of these macroporous packings. The TEM images presented in Figure 5A and B, respectively, of the 1000 and 4000 Å materials show that a large fraction of the pores are through-pores (500 Å were not analyzed).

Electrochromatography. Chromatographic results for the 500, 1000, and 4000 Å nominal pore diameter packings at various

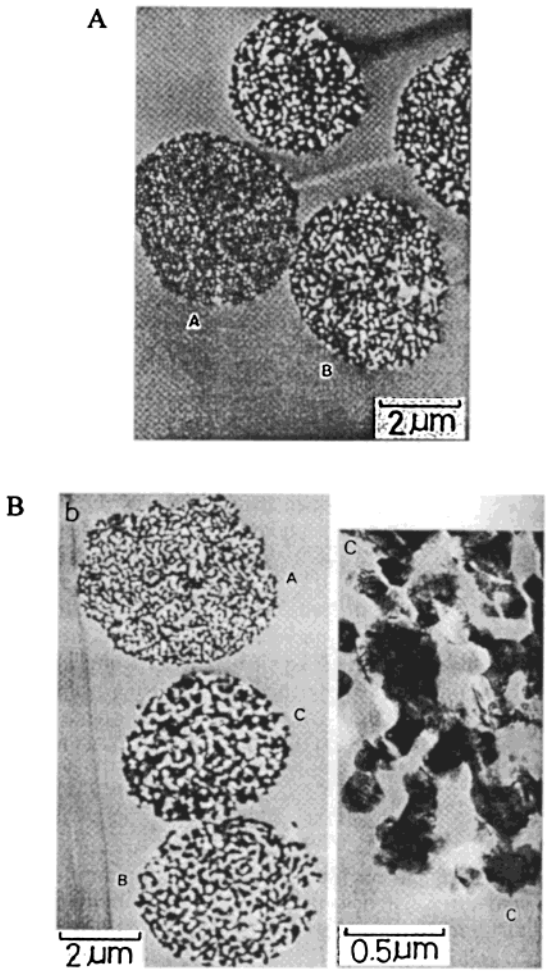

Figure 5. Transmission electron micrographs of 5 μm d_p Nucleosil particles. (A) 1000 Å, (B) 4000 Å. The letter notation in the insets indicates the types of particles that constitute each packing material. From ref 17 with permission from Elsevier Science.

buffer concentrations are summarized in Figures 6 and 7 in which reduced plate height h ($h = H/d_p$) is plotted against reduced velocity v ($v = \mu d_p/D_m$). To best illustrate the trends present in these data sets, the results are presented in two ways. In Figure 6, findings for the three types of packings at 1, 50, and 100 mM Tris are plotted as series and grouped according to Tris concentration, while Figure 7 shows the full data set with buffer concentrations plotted as series and grouped according to nominal pore size. Several interesting features of these curves warrant an in-depth examination of the data. At the lowest Tris concentration, 1.0 mM, the curves differ in their shapes as well as relative positions on the *y*-axis. For the 500 and 1000 Å columns, a minimum in the curves is observed at $h \approx 1.2$ and 0.9 and $v \approx 3.6$ and 5.0, respectively. The 4000 Å capillary exhibited not only lower plate heights over the entire velocity range but a flatter curve at high v with a barely discernible minimum at $h \approx 0.6$, $v \approx 6.8$. In view of the fact that the Nucleosil materials are of the same 7 μm nominal d_p (verified by SEM), these results suggest that there was some extent of intraparticle flow occurring at buffer concentrations as low as 1.0 mM. It should be noted that the maximum velocity in each of these data sets was obtained at the highest obtainable electric field strength (i.e., a potential of +30 kV applied

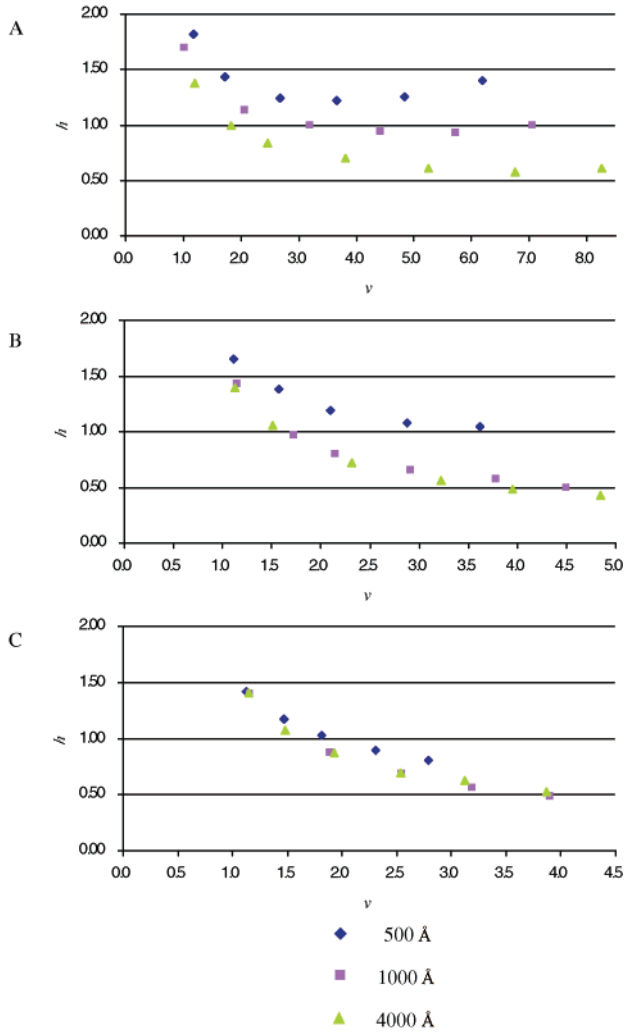

Figure 6. Experimental rate curves: (A) 1.0, (B) 50, and (C) 100 mM Tris.

to the shortest length of column possible with the instrument used).

As the buffer concentration was increased to 10 mM, no improvement in plate height was seen for the 500 Å column (there was actually a modest increase in h_{min}). In addition, the shape of the curve is roughly the same as that for the 500 Å−1.0 mM Tris data set. For the 1000 Å column, h_{min} decreased slightly to ~0.8. The 4000 Å column, however, showed no plate height minimum up to $v \approx 7.0$, at which $h \approx 0.4$. The shape of this curve differs slightly from the 4000 Å−1.0 mM data set, with a lower h at a given v, especially at $v > 3.0$. Importantly, no minimum was observed in this curve. It can be inferred from the shape of this curve that a minimum, if it exists, will lie somewhat to the right of (i.e., at a higher velocity than) that observed for the 1.0 mM Tris buffer. Again, the limit of 30 kV, imposed by the instrument, precluded the investigation of higher velocities.

At 25 mM Tris, the curve generated by the 500 Å data set is scarcely different from the 500 Å−1.0 mM curve. Although the lowest observed h for the 4000 Å−25 mM curve was approximately equal to that of the 4000 Å−10 mM curve ($h \approx 0.4$), it was achieved at a lower v ($v \approx 5.6$ vs 7.0). Thus, the shape of the curve again changed as Tris concentration was increased. A similar change in curve shape was observed for the 1000 Å−25 mM data set where, relative to the 1000 Å−10 mM and 1000 Å−1.0 mM data, the curve is shifted to lower h values with the divergence increasing with v. Additionally, the 1000 and 4000 Å curves begin to overlap, in particular at lower values of v, which suggests that, on going from 10 to 25 mM Tris, the extent of change in the curve shape was greater for the 1000 Å column.

Increasing the Tris concentration to 50 mM resulted in a similar change in the shape of the 500 Å curve. The lowest observed reduced plate height of 1.0 was obtained at the maximum achievable reduced velocity, $v \approx 3.6$ with the curve bearing no observable h_{min}. With respect to the 1000 Å−50 mM and 4000 Å−50 mM data sets, further small changes in the curves, continuations of the same trend, were observed. Interestingly, the 1000 Å−50 mM and 4000 Å−50 mM curves are virtually superimposable, the latter with $h \approx 0.4$ at a relatively low $v \approx 4.8$.

At the highest Tris concentrations (75 and 100 mM), no noticeable changes in the 1000 and 4000 Å curves were observed. The 500 Å−75 mM curve, however, showed a marked shift to lower h values, toward the 1000 Å−75 mM and 4000 Å−75 mM curves. This again appears to be an extension of the previous trends. At the maximum velocity $v = 2.8$, the reduced plate height was ~0.85, a significant decrease relative to results for the same column with 1.0 mM Tris. A further shift toward lower h and convergence with the larger pore sizes is seen for the 500 Å−100 mM curve, where $h \approx 0.80$ was obtained at a maximum velocity of 2.8.

To summarize, at the most dilute buffer concentrations (i.e., 1.0 and 10 mM), the ability of the columns to generate a low plate height ranked according to the nominal pore size of the packing ($h_{500\ Å} > h_{1000\ Å} > h_{4000\ Å}$). The curves also exhibited different shapes, particularly in the high-velocity regions, with the larger nominal pore sizes having the more shallow slopes. Increasing the Tris concentration resulted in changes in the shapes of the curves generated for each packing material, with the 1000 and 4000 Å curves starting to converge at a Tris concentration of 50 mM. Here a limiting point was reached for these larger pore packings, as no changes were apparent as Tris was increased to 75 and 100 mM. Further changes, however, were observed for the 500 Å curves, which at 100 mM Tris had closely approached the curves for the larger pore sizes. It should be noted also that linear velocity versus field strength plots were obtained for each condition in the study. Thus, Joule heating effects, even at 100 mM Tris, were determined to be negligible.

These data and the observed trends provide evidence for electroomosis in the pores of these particles. Moreover, these results suggest that (1) a fraction of macropores exists in the 1000 and 4000 Å packings capable of supporting electroosmosis with Tris concentrations as low as 1.0 mM and (2) the fraction supporting EOF can be increased, up to a point, by increasing the buffer concentration, thereby compressing the double layer.

The limiting behavior of the h versus v curves can be rationalized as follows. Each type of packing possesses a certain fraction of macropores that can support EOF under the conditions of the experiment. At the most dilute buffer concentration, the benefit of lower h due to intraparticle flow, if any, will be most pronounced for the packing having the greatest fraction of the largest pores, in this case the 4000 Å packing. When the buffer is made more concentrated, compressing the double layer, improve-

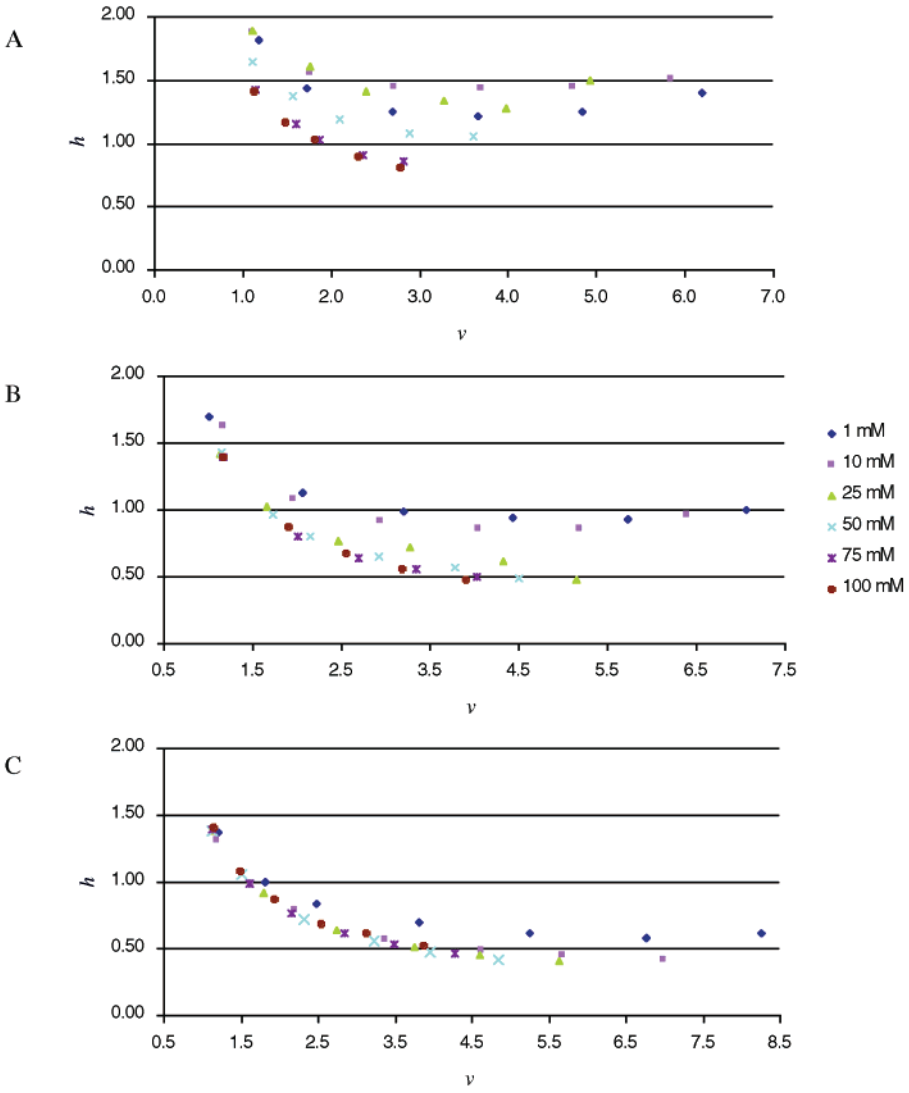

Figure 7. Experimental rate curves: (A) capillary 1−500 Å pores, (B) capillary 2−1000 Å pores, and (C) capillary 3−4000 Å pores.

ments in h will be made as a greater number of smaller diameter pores can now support EOF. However, a point is reached at which no further reduction in h is possible: there is now flow in a significant fraction of the available macropores. The buffer concentration at which this limiting point is reached is necessarily dependent upon the pore size distribution and average pore size of the packing; the larger pore media reach a limit at a lower buffer concentration relative to smaller pore sizes.

Application of Model. For illustrative purposes, values of the weighting factors χ_v and χ_e obtained for three representative pore size intervals, 100, 1000, and 4000 Å, at different eluent buffer concentrations are provided in Table 3. Values of δ derived using eq 2 for the range of Tris concentrations used are shown in Table 4. In these calculations, a dielectric constant (ϵ_r) of 45 was assumed for each eluent.[18] The pore diameter intervals and associated weighting factors shown in Table 3 are 3 out of the 995 total intervals that represent the intraparticle pore space considered in the model. It is at the lowest buffer concentration where the differences in the packings are most pronounced. Therefore, a plot of the dimensionless lumped weighting factor χ_I for the various intraparticle pore intervals at 1.0 mM Tris is presented in Figure 8 to better illustrate the model.

The $d_{p,eff}$ values generated by the model are presented in Table 5. It can be seen that the general trends observed in the experimental data are reflected also in the $d_{p,eff}$ values. For example, at the lowest Tris concentration, 1.0 mM, the model predicts a considerably higher contribution of intraparticle EOF for the 4000 Å packing relative to the 500 Å, manifest in a smaller $d_{p,eff}$ value. In addition, $d_{p,eff}$ for the 1000 Å media lies between the 500 and 4000 Å. Examining once again the experimental data in Figures 6 and 7, it is found that the model correctly predicts the trend $h_{500\ Å} > h_{1000\ Å} > h_{4000\ Å}$ observed for 1.0 mM Tris. As Tris concentration is increased to 100 mM, the model further predicts the observed convergence of the rate curves for the three packing types. That the 1000 Å packing possesses a slightly smaller $d_{p,eff}$ than the 4000 Å material at this Tris concentration is a consequence of the preponderance of 800−1200 Å pores in the former, which at higher Tris concentrations can support EOF, thereby weighting the average toward a smaller $d_{p,eff}$.

The $d_{p,eff}$ values generated by the model help to illustrate some practical implications of perfusive electroosmosis not obvious from

(18) Schwer, C.; Kenndler, E. *Anal. Chem.* **1991,** *63*, 1801−1807.

Table 3. Weighting Factors χ_v, χ_e, and χ_I for 3 of the 995 Intraparticle Pore Size Intervals Used in the Estimation of $d_{p,eff}$

nom pore diam (Å)	pore interval (d_{ch}) (Å)	χ_v	χ_e			χ_I			ϵ_{pore}
			1.0 mM	50 mM	100 mM	1.0 mM	50 mM	100 mM	
500	100	0.0098	0.006	0.229	0.353	5.9×10^{-5}	2.2×10^{-3}	3.5×10^{-3}	0.51
	1000	0.0027	0.345	0.878	0.913	9.3×10^{-4}	2.4×10^{-3}	2.5×10^{-3}	
	4000	6.0×10^{-5}	0.789	0.969	0.978	3.1×10^{-5}	3.8×10^{-5}	3.8×10^{-5}	
1000	100	0.0059	0.006	0.229	0.353	3.5×10^{-5}	1.4×10^{-3}	2.1×10^{-3}	0.54
	1000	0.0031	0.345	0.878	0.913	1.1×10^{-3}	2.7×10^{-3}	2.8×10^{-5}	
	4000	0.0015	0.789	0.969	0.978	1.2×10^{-3}	1.5×10^{-3}	1.5×10^{-3}	
4000	100	0.0039	0.006	0.229	0.353	2.3×10^{-5}	8.9×10^{-4}	1.4×10^{-3}	0.52
	1000	0.0014	0.345	0.878	0.913	4.8×10^{-4}	1.2×10^{-3}	1.3×10^{-3}	
	4000	0.0019	0.789	0.969	0.978	1.5×10^{-3}	1.8×10^{-3}	1.9×10^{-3}	

Table 4. Double-Layer Thickness (δ) Values at the Tris Concentrations Employed in the Study Calculated As Described in the Text[a]

nom Tris concn (mM)	δ (Å)	nom Tris concn (mM)	δ (Å)
1.0	224	50	31.6
10	70.7	75	25.8
25	44.7	100	22.4

[a] Note: δ values reflect 1:5 dilution of Tris in acetonitrile.

Table 5. Values of $d_{p,eff}$ Generated by the Model

nom pore diam (Å)	$d_{p,eff}$ (μm)					
	1.0 mM	10 mM	25 mM	50 mM	75 mM	100 mM
500	5.81	4.84	4.57	4.40	4.32	4.26
1000	5.16	4.39	4.21	4.09	4.02	3.98
4000	4.96	4.37	4.24	4.15	4.11	4.08

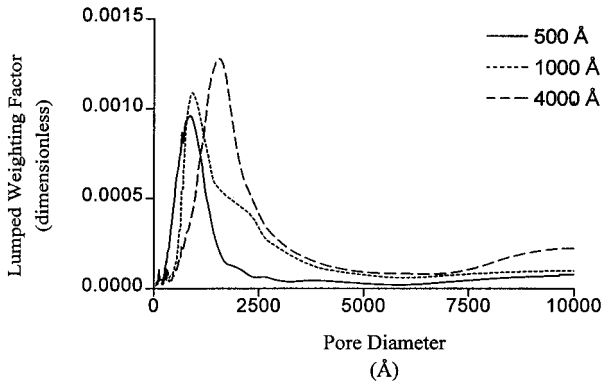

Figure 8. Lumped weighting factor χ_I versus pore diameter. Pore diameter values represent the midpoints of the appropriate intervals determined as described in the text. χ_I values for the interstitial region (not included on the graph) are 0.50 (500 Å), 0.44 (1000 Å), and 0.46 (4000 Å)

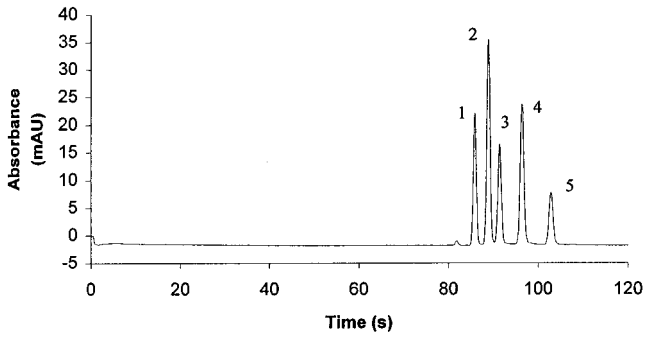

Figure 9. Separation of polyaromatic hydrocarbons on capillary 3 (4000 Å pores). Peaks: (1) naphthalene (308 000 plates m^{-1}), (2) acenaphthene (289 000 plates m^{-1}), (3) anthracene (272 000 plates m^{-1}), (4) pyrene (264 000 plates m^{-1}), and (5) chrysene (237 000 plates m^{-1}). Conditions: mobile phase (20:80) 10 mM Tris pH 8.0/acetonitrile; separation voltage, +30 kV; $\mu = 3.1$ mm s^{-1}; injection +3 kV, 3 s; detection, UV 230 nm; capillary dimensions, as indicated in Table 1; sample, 75 μg/mL each compound in mobile phase.

the experimental data alone. In CEC, as in most chromatographic techniques, it is desirable not only to achieve high efficiencies but to do so in a minimal amount of time. With the larger pore packings (1000 and 4000 Å), there is only a marginal decrease in $d_{p,eff}$ as Tris concentration is increased above 50 mM. However, EOF velocity decreases as the square root of buffer concentration, thus limiting the achievable linear velocity. There exists, then, a set of conditions that yields the optimum combination of speed and efficiency. Recall from the rate curves in Figure 7 that no minimum was observed for 4000 Å packing for Tris concentrations as low as 10 mM. At 10 mM Tris, a very low h of 0.42 was obtained at a relatively high v of 7.0, at which the maximum potential of 30 kV of the instrument was applied. Clearly, this set of conditions offers the best combination of speed and efficiency, as evidenced by the separation of polyaromatic hydrocarbons (PAHs) in Figure 9.

One advantage to expressing the contribution of intraparticle flow in these macroporous packings in terms of an effective particle diameter, rather than effective channel diameter, is the ability to generate rate curves in more familiar terms. In addition, reduced parameters based on $d_{p,eff}$ should allow for a more accurate assessment of the relationship between h and v, than do parameters based on nominal d_p.

To that end, the experimental rate curves obtained for the three columns were replotted with h and v values determined by scaling to the appropriate $d_{p,eff}$ values. These are shown in Figure 10.

If the improvements in plate height with increasing perfusive character of the packings were attributable solely to a decrease in effective particle diameter, the rate curves of the "effective" reduced parameters for a given column should be quite similar regardless of Tris concentration. That is, normalization of plate height and linear velocity to $d_{p,eff}$ should account for the observed differences in efficiency. This, however, is not observed. Inspection of the curves in Figure 10 reveals that the curves exhibit a trend similar to the "uncorrected" data shown in Figure 7. With the

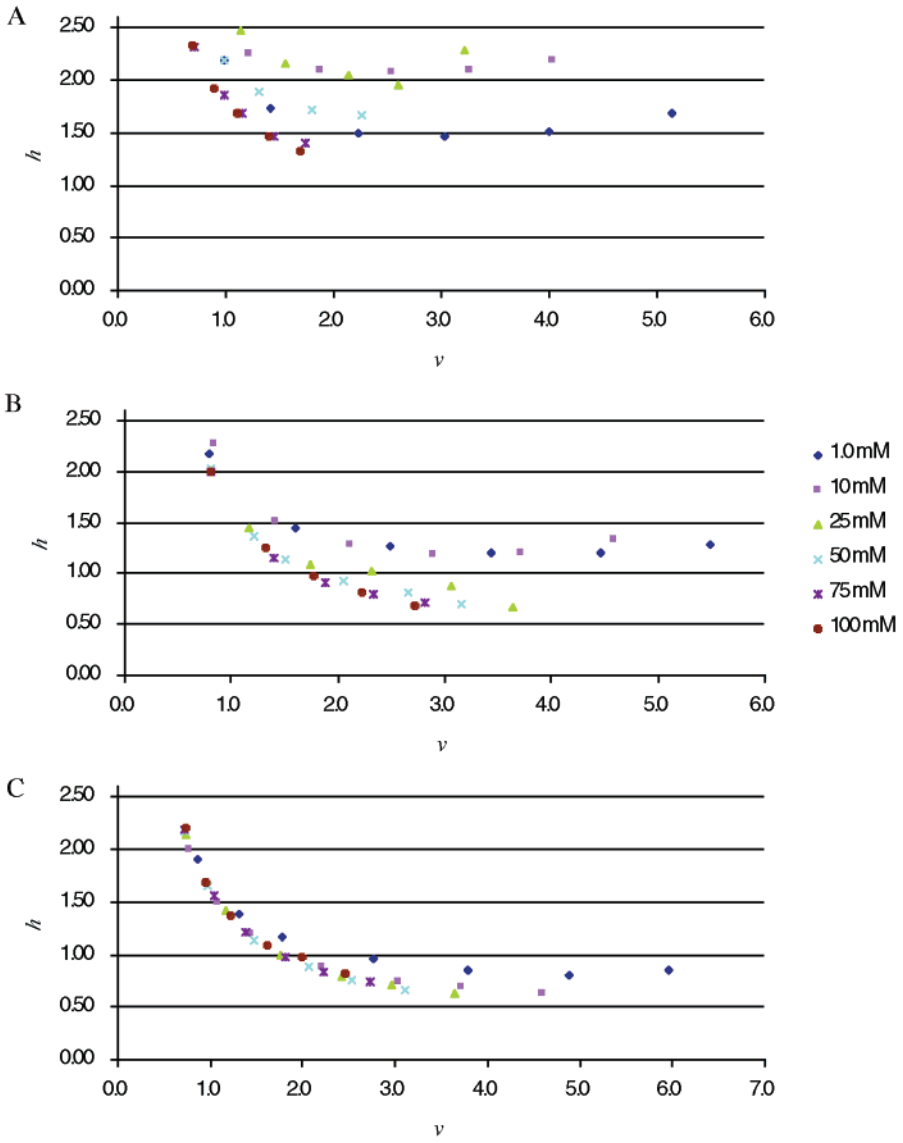

Figure 10. Rate curves with reduced parameters calculated based on $d_{p,eff}$: (A) capillary 1, 500 Å pores; (B) capillary 2, 1000 Å pores; (C) capillary 3, 4000 Å pores.

exception of one anomalous data set, the 500 Å−1.0 mM Tris, the curves tend toward lower h values as Tris concentration increases. It is interesting to note that the degree of difference in the "effective" rate curves in Figure 10 appears to correlate inversely with the pore size of the packing. That is, the differences are most pronounced for the 500 Å material and least so for the 4000 Å. As shown previously, the 4000 Å packing exhibited the highest perfusive character at the lowest Tris concentration of 1.0 mM; it is possible that larger differences exist at lower buffer concentrations.

It can be concluded from these data that reductions in $d_{p,eff}$ with increased perfusion alone do not explain the observed plate height improvements. The differences in the rate curves in Figure 9 imply that increasing the perfusive character of the packing causes the column to take on the characteristics of not only a bed of smaller particles but a bed of more tightly packed particles. The Knox equation, $h = Av^{1/3} + B/v + Cv$, is commonly used to describe h versus v behavior in packed column liquid chromatography.[12] The A term in this expression includes the coupled effects of eddy diffusion and mobile-phase mass transfer, the B term longitudinal molecular diffusion, and the C term stationary phase and stagnant mobile-phase mass transfer effects. It is evident from the curves in Figure 10 that differences in the magnitude of plate height coefficients A and C exist (the curves converge in the low-velocity B term-dominated region). Although a lower C term with increased perfusion is not surprising owing to stagnant mobile-phase effects, the shapes of the curves and range of velocities tested suggest that the disparity in the curves is due primarily to differences in the A term of the plate height equation. Differences in the A term may arise from geometrical effects in the intraparticle flow channels, perhaps the result of lower tortuosity factors for the wider pore media. In such cases, a decreased multipath (eddy diffusion) contribution to h may result. Values of the plate height coefficients can be obtained by fitting the rate curves to an empirical equation, usually the Knox equation. However, to yield meaningful values requires a wider range of velocities (i.e., the inclusion of higher velocities) than possible here. In principle, if $d_{p,eff}$ is precisely known, improvements in the plate height coefficients, if any, can be discerned.

CONCLUSION

Improved chromatographic efficiency with increasing perfusive character of the packing medium was observed with commercially available reversed-phase packings and typical CEC eluents. Experimental rate curves obtained for the larger pore packings, 4000 and 1000 Å Nucleosil, suggest the presence of intraparticle EOF at buffer concentrations as low as 1.0 mM. From a practical point of view, the experimental data indicate that optimum chromatographic performance (i.e., speed and efficiency) can be achieved with macroporous packings and relatively low buffer concentrations.

The extent of intraparticle EOF under a range of eluent conditions was estimated and expressed in terms of an effective particle diameter. Although this model predicts the trends in the data, it is difficult to evaluate the accuracy of the $d_{p,eff}$ values it yields. Rate curves of reduced parameters calculated with $d_{p,eff}$ values indicate that, in addition to a smaller effective particle diameter, wide-pore media operated under perfusive conditions may yield lower A term (tortuosity dependent) contributions to plate height. The phenomena observed here warrant further study in order to provide a more thorough understanding of the effect of intraparticle EOF on efficiency in CEC.

ACKNOWLEDGMENT

The authors thank Dr. Al Soeldner at the Oregon State University Electron Microscopy Facility for his assistance in obtaining the SEM images.

LIST OF SYMBOLS

a	channel radius
C	molar concentration of electrolyte
d_{ch}	channel diameter
$\overline{d_{ch}}$	weighted average channel diameter
D_m	diffusion coefficient of solute in mobile phase
d_p	particle diameter
$d_{p,eff}$	effective particle diameter
E	electric field strength
F	Faraday's constant
f_i	volume fraction of interval i
H	plate height
h	reduced plate height
I_0	zero-order Bessel function of the first kind
I_1	first-order Bessel function of the first kind
R	gas constant
T	temperature
V	EOF velocity (point)
$\bar{V}$	cross sectional average EOF velocity
V_{rel}	relative EOF velocity
$\bar{V}_\infty$	cross sectional average EOF velocity at large κa
v	reduced velocity
χ_e	relative EOF weighting factor
χ_l	lumped weighting factor
χ_v	volume fraction weighting factor
δ	double-layer thickness
ϵ_0	permittivity of vacuum
ϵ_i	interstitial porosity
ϵ_p	particle porosity
ϵ_{pore}	fraction of column void volume contributed by intraparticle pores
ϵ_r	dielectric constant of mobile phase
ϵ_{tot}	total column porosity
κ	reciprocal of double-layer thickness
η	mobile-phase viscosity
μ	mobile-phase linear velocity
ζ	zeta potential

Received for review May 23, 2000. Accepted July 16, 2000.

AC0005969